IEEE Access
Multidisciplinary | Rapid Review | Open Access Journal

Received October 4, 2021, accepted October 17, 2021, date of publication October 22, 2021, date of current version October 28, 2021.

Digital Object Identifier 10.1109/ACCESS.2021.3122123

A Novel Current Control Method Based on Dual-Mode Structure Repetitive Control for Three-Phase Power Electronic Load

ZHENG ZHANG, XINGHUA LIU, YUE ZHANG, CHONGBING ZHANG, AND WANGMIN DENG
School of Mechanical Engineering, Beijing Institute of Technology, Beijing 100081, China
Corresponding author: Zheng Zhang (zhz_bit@163.com)

ABSTRACT The test platforms of motor driver are relatively expensive, high energy consumption, complex mechanical structure, and not readily available. A three-phase power electronic load of simulated permanent magnet synchronous motor is used to eliminate the risk associated with the performance testing of motor driver, without complex mechanical system. This equipment not only can simulate a variety of load characteristics, but also has the ability to recover energy with little loss and high power factor. In this work, a novel current tracking control strategy based on dual-mode structure repetitive control (DMRC) is proposed to improve the tracking accuracy of alternating current. Compare to control strategy operated in the d-q coordinate system, the proposed control strategy can direct track sine wave commands on the stationary α-β coordinate system, which is easier to implement with fewer intermediate coordinate transformation in practice. An inductor-capacitor-inductor (LCL) filter is used to interface the voltage source converter (VSC) and the tested inverter in the three-phase electronic load system. Adjusting the odd-harmonic gain and even-harmonic gain of DMRC controller can effectively suppress the current harmonics. Furthermore, the comparative evaluation of DMRC, repetitive control and conventional PI control is conducted to verify the superiority of DMRC at different AC voltage frequency of tested inverter. The simulation has been carried out on three-phase power electronic load. As a result, the proposed method can achieve low total harmonic distortion (THD) (<1.8%) of AC current, It can provides nearly 20% reduction of THD in phase current when compared with PI controller.

INDEX TERMS Repetitive control (RC), voltage source converter (VSC), current harmonic, electronic load.

NOMENCLATURE

$U_{\_dc}$, U_{dc_ref}	The dc voltage, dc reference voltage.
U_{E_ref}	The dc voltage of Test-Inverter
$E_{\_abc}$, Ea, Eb, Ec	Test-inverter output voltage, voltage on abc-reference frame,
$E\alpha$, $E\beta$	Test-inverter output voltage on $\alpha\beta$-reference frame,
U_{c_abc}, Ua, Ub, Uc	LCL filter capacitor voltage, voltage on abc-reference frame,
$I_{\_ref}$, $I_{\_abc}$,	Test-inverter output reference current, actual current,
$I\alpha\_ref$, $I\beta\_ref$	reference current on $\alpha\beta$-reference frame,
Ia, Ib, Ic	Test-inverter output current on abc-reference frame,
$I\alpha$, $I\beta$	Test-inverter output current on $\alpha\beta$-reference frame,
L1,R_L,	Simulation converter side inductance, parasitic resistances of L1
L2, R_E.	Test-Inverter side inductance, parasitic resistances of L2.
Cf, R_C.	Capacitance of LCL filter, parasitic resistances of Cf.
θ.	Phase angle of phase A voltage from phase lock loop.
I_{e_abc}, I_{e_a}, I_{e_b}, I_{e_c}.	Simulation converter input current, current on abc-reference frame,
da, db, dc.	PWM signals of simulation converter on abc-reference frame,
d_α, d_β.	PWM signals of simulation converter on $\alpha\beta$-reference frame.
$G_p(z)$	Transfer function of simulation converter and LCL filter.

The associate editor coordinating the review of this manuscript and approving it for publication was Padmanabh Thakur.

$G_c(z)$	Transfer function of the conventional PI controller.
$Q(z)$	Low pass filter transfer function or a constant value.
$G_f(z)$	The inverse function of Gp(z).
$D(z)$	The disturbance.
$I(z)$	Test-inverter output current.
$I_{ref}(z)$	Test-inverter output reference current.
$E(z)$	The error of current between Iref(z) and I(z).
$H(z)$	The conventional control system transfer function.
$G_{dr}(z)$	Dual-mode-structure RC controller transfer function.
$G_{ogm}(z)$	An even-harmonic signal generator transfer function.
$G_{egm}(z)$	An odd-harmonic signal generator transfer function.
k_o	An odd-harmonic gain.
k_e	An even-harmonic gain.
k_r	The conventional repetitive controller gain.
f_s	The sampling rate.
T_s	The sampling period.
f_0	Fundamental reference frequency of the signals Iref(z).
ε	A positive constant.
$\Delta(z)$	The uncertainties.
$M(z)$	The error transfer function from reference current signal Iref(z) minus disturbance signal D(z) to current steady-state error E(z).
N	Number of samples in one repetitive reference period.
L	The delay time interval of both controller and plant.
ξ	Damping ratio
K_d	Damping coefficient

I. INTRODUCTION

Validation and test of driving inverters should be carried out to ensure appropriate efficiency and performance in the final stage of development of three-phase tested power supply equipment [1]. Generally, in terms of flexibility, cost and time savings, three-phase power electronic load is an emerging method for validation of driving inverters and control schemes [2]–[10]. Recently, three-phase power electronic load has been proposed by academic research to simulate the behavior of the actual machine when connected to grid or a voltage source inverter (VSI). The control algorithms and driving inverters can be tested with the use of three-phase electronic load to provide different load characteristics [4], [7], [11]–[13].

Three-phase power electronic load has received significant attention and increasingly recognition as an effective approach for testing driving inverters in recent years [4], [9], [16], [18]. The authors of [4] presented a real-time real-power electrical machine emulator, which is designed to simulate the behavior of a low-voltage induction motor coupled with a mechanical load. The researchers have studied many aspects of the three-phase electronic load system, such as the power amplifier topology, the structure and the characteristics of coupling filter [16], [18]. In [16], the LCL-type coupling filter appeared to be the best solution, through the comprehensive analysis and comparison of LCL-type filter and the simple inductor filter generally used in [18]. However, high-power amplifiers based on a voltage source inverter could result in significant precision errors and even instabilities, due to the discrete voltage levels producing by the power electronics switches [14].

When the three-phase power electronic load emulate the machine, the more important considerations are the coupling or interface components connecting the electronic load and the tested inverter, machine models and the control method used by the three-phase electronic load. Many studies have been done by researchers on these issues. There has been some work addressing conflict occurred in control between the inverter and the three-phase electronic load in the literature [2]–[5], [8], [15]. When the driving inverter acts as a voltage source and the electronic load typically works in current controlled mode, there is no conflict occurred in control between them. But the tested inverter and the three-phase electronic load working in current control mode at the same time, could possibly lead to control oscillations [3], [5]. Refs. [2]–[5], [8], [15] try to discuss and research different ways to avoid damaging the stability of the electronic load system. To avoid the controlled mode conflict, the accuracy of the emulation reduces significantly due to modified and simplified the machine model of electronic load system [3], [5]. Such simplified machine models can meet the accuracy requirements of steady state conditions but reducing the degree of fidelity in transient emulation.

When performing the three-phase electronic load system, another important consideration is the coupling or interface components connecting the three-phase electronic load and the tested inverter. Choosing an inductive filter (L) is a well-reported method for the resulting simplicity of the three-phase electronic load system. Using a simple inductive-filter (L) as an interconnection between the tested inverter and electronic load has been discussed in significant detail in [9], [10], [14], and [45]. A coupling inductor-capacitor (LC) filter network is a low pass filter placed at the output of the VSC of electronic load. The LC network filters some of the switching frequency harmonics generated due to the pulse width modulation (PWM) at the terminals of VSC [6]. The current of the inductor L in LC network appears to be smoother when compared to the current in the simple link-inductor filter in [23]. However, current error is introduced between the inverter terminals and the output of the VSC of electronic load. An inductor-capacitor-inductor (LCL) output filter is used to avoid conflicts with the current controller in the inverter, overcoming the shortcomings of the two filters mentioned above [23]. It has the advantages of low cost, small size and fast dynamic response.

Furthermore, the interface components arrangement of LCL filter requires damping resistances to avoid resonance. Based on the three-phase electronic load system, [2] provides a novel induction machine emulator to test the driving inverters. The output of the emulator is connected to the inverter via a transformer-based LCL-type coupling network.

The performance of a three-phase electronic load system is tested by using a PI-controller in the abc-reference frame in [1] and [4]. A control approach in a three-phase induction machine emulator (IME) testing platform runs in the synchronously rotating reference dq coordinates frame utilizing three-phase electronic load system [2]. The capability of a current optimal control method using a linear quadratic regulator is presented and investigated in the three-phase electronic load system [7]. An induction motor emulator considering the main and leakage flux saturation by using the three-phase electronic load system is researched, which employed a proportional-resonant current controller in the abc-frame [8]. A three-phase electronic load system simulating the performance of PMSM under both healthy conditions and during inter-turn stator winding faults is investigated in a safe and inexpensive environment [24]. The high-performance model predictive current control (MPCC) is used for a programmable AC load (PEAL) [44]. In each period, switching state that minimizes the cost function is based on input current of PEAL and applied to the converter. In [48], the feedback controller used in load simulator is a QPR controller to tracking AC current. In relatively recent development, repetitive control has been attracting increased attention in the academic and industry communities [20]–[22]. The repetitive control (RC) technique, using the internal model principle [25], is an effective tool to track periodic reference signals and to minimize steady-state tracking error and total harmonic distortion (THD). Nowadays, it has been widely applied to various aspects [26]–[30], such as active power filter [27]–[28] and voltage source inverter (VSI) [29]–[30]. A nonlinear disturbance observer (NDO) based sliding-mode control [47] is applied to power electronic loads to emulate constant power loads (CPLs). A hybrid five-level voltage source inverter (VSI) [46] is designed and applied to simulate various static load behaviors. In [43] a conventional RC is designed and applied to the AC electronic load with energy recycling. Through the input current precision of load simulator is greatly improved, the response of traditional RC is slow and the delay is more than one basic cycle.

To further improve the control performance of RC, a dual-mode-structure RC (DMRC) [31], [37] is proposed, which comprises of two paralleled signal generators. The plug-in DMRC [38] is proposed to eliminate the total harmonic distortion under nonlinear load condition. The results show the DMRC achieves a faster error convergence rate than the conventional RC does. A second-order DMRC proposed in [39] introduces fractional delay filters based on Lagrange-interpolation to improve the current suppression accuracy in magnetically suspended rotor (MSR) systems.

A 3/2-order fractional-order DMRC scheme with a three-parallel structure for magnetically suspended rotor systems is proposed in [41] dealing with harmonic currents caused by errors of displacement sensor and mass imbalance. An approach [42] which permits the application of the fuzzy repetitive controller in the Takagi–Sugeno (T–S) fuzzy observer-based controller design to deal with the periodic tracking control problem is based on introducing an additional parameter in the fuzzy Lyapunov functional for nonlinear systems.

The most popular current control methods for electronic AC load are proportional-integral (PI) control [49] and conventional repetitive control [42]–[43], [45], [48]. The PI control method is suitable for balance system in the synchronous reference frame. However, it cannot work well when the electronic AC load simulates nonlinear load and unbalance load. Conventional RC is an effective solution for eliminating the periodic errors and tracking the periodic reference signal. Due to the digital sampling and PWM delays in the digital control system, the phase lag of the conventional RC reduces the tracking accuracy and convergence rate. Comparing to a close-to-unity constant [45], a well-designed low pass filter Q(z), is easier to enhance the robustness of the overall plug-in DMRC system.

A digital dual-mode-structure repetitive control approach is proposed in [40] for the single-phase shunt active power filter (APF). It can improve the tracking ability of current and eliminate high order harmonic. Although the DMRC control approach can get promising results, it remains the problem on how to further effectively improve the accuracy of three-phase voltage source converter. Furthermore, a high-performance of DMRC for three-phase power electronic load system needs to be developed. In this paper, a plug-in DMRC scheme is presented for the three-phase power electronic load system to suppress the tracking error and current harmonic on the $\alpha\beta$ stationary reference frame. The plug-in DMRC method can reduces the delay time to N/2 sampling intervals when then delay time of CRC is N sampling intervals. Without increasing complexity, the plug-in DMRC method provides a universal framework for developing various RC controllers, such as CRC (when $k_o = k_e = 1/2$) and odd-harmonic repetitive control (OHRC) (when $k_o \neq 0$ and $k_e = 0$). For a three-phase AC systems with abundant $6k \pm 1$th order harmonics, the plug-in DMRC method provides a superior control performance when increase the proportion of gain ko and reduce the proportion of gain k_e.

The plug-in DMRC occupies the same memory cells as CRC. When compared with CRC, It can significantly improve the current tracking performance without additional complexity design. Stability analysis and design process are derived for the plug-in DMRC method in this paper. A simple and efficient linear phase lead compensation is designed for the plug-in DMRC system. Simulation verification of the proposed plug-in DMRC method on the three-phase power electronic load system is carried out to demonstrate the effectiveness of the proposed current control method under various

reference current frequencies. Comparisons of PI control, CRC and DMRC are presented under different AC voltage frequency. To eliminate the periodic disturbances, this paper also investigates the relationship between odd-harmonic gain and even-harmonic gain of the dual-mode-structure repetitive control in the three-phase power electronic load system. The plug-in DMRC offers a promising solution to further improve the performance of RC.

The organization of this paper is as follows. The structure of the three-phase electronic load system and its conventional PI control strategy has been presented in Section II. The Section III presents the plug-in DMRC controller design for the three-phase electronic load system. Simulation comparisons of conventional PI control, CRC and DMRC are presented in Section IV. The conclusion of the whole paper has been summarized in Section V.

II. THREE-PHASE POWER ELECTRONIC LOAD SYSTEM

A. STRUCTURE OF THREE-PHASE POWER ELECTRONIC LOAD

The diagram of the three-phase power electronic load system is depicted in Fig. 1. The simulation converter includes a two-level six-switch bridge-type voltage source converter (VSC) [2], [4], [8]. $L1$, $L2$ and C_f are the three-phase power electronic load-side inductance, the driving inverter-side inductance, and the capacitance of the LCL filter, respectively. The test-inverter (driving inverter) topology used in this paper is a standard two-level VSC as well. A LCL filter is used as an interface element between the driving inverter and the proposed three-phase power electronic load.

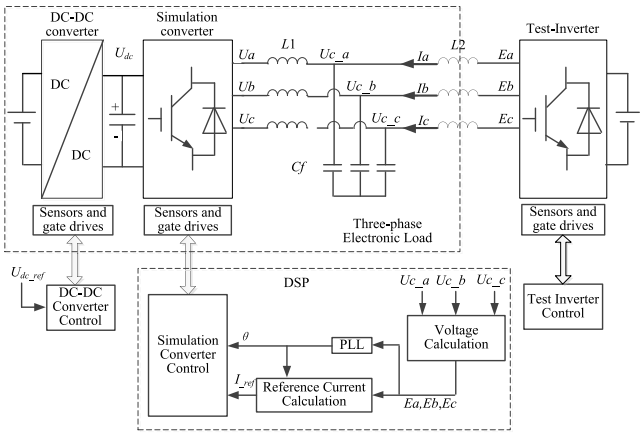

FIGURE 1. Structure diagram of the three-phase power electronic load system.

The objective of the non-isolated bidirectional DC-DC converter control is to ensure that the emulating converter achieving the desired response and control the bidirectional power flow from or to the simulation converter. The controller design for the non-isolated bidirectional DC-DC converter is not discussed here, as it is quite well established [32]–[34]. The non-isolated bidirectional DC-DC converter control should be as fast as possible to maintain a fixed DC link voltage of the three-phase electronic load. The control algorithms for the non-isolated bidirectional DC-DC converter, the simulation converter and the driving inverter are implemented in DSP. The conventional PI control algorithm combining with inverter-voltage feed-forward strategy can be illustrated within switching cycle of 100us time frame inside the current controller in Fig. 2 (a). The control strategy includes coordinate conversion, PLL and conventional PI control block. If the output voltage of the test-inverter is rectangular wave, according to Kirchhoff's current law and voltage law, the output voltage of test-inverter can be approximately calculated by $E_{\_abc} \approx U_{c\_abc} + R_E^* I_{\_abc}$.

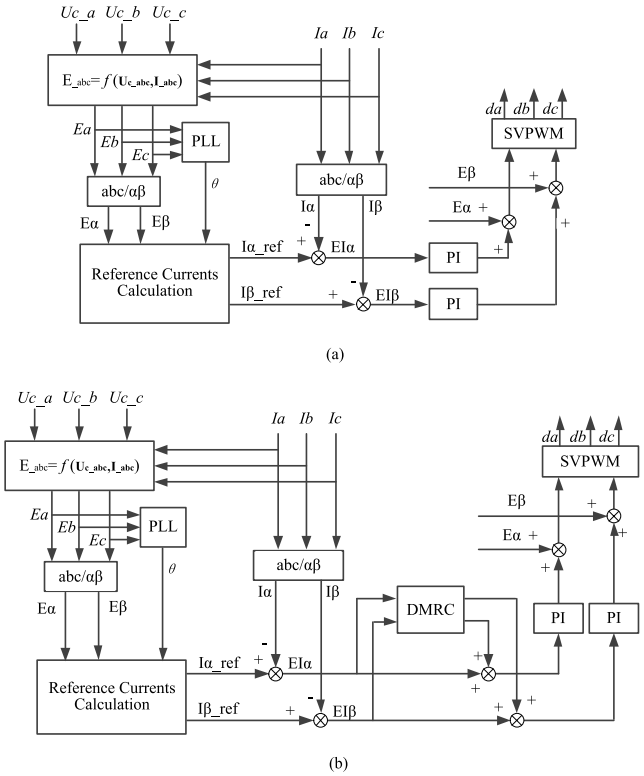

FIGURE 2. The three-phase power electronic load current control method in α-β reference frame. (a) Under the conventional PI control strategy, (b) under CRC strategy.

The test-inverter runs on a separate controller and has no interacted with the three-phase power electronic load controller in Fig. 2. The current control algorithm requires the feedback of the input currents Iα, and Iβ in the three-phase power electronic load system. The three-phase actual currents drawn from driving inverter must be controlled to be approximately equal to the output of reference currents calculation Iα_ref, and Iβ_ref calculated. The difference between the three-phase actual currents and the reference current is the input of the current controller. The PWM signals are modulated and sent to the gate drives of the simulation converter.

Fig. 3 shows the basic computer flow chart for the proposed current control method in three-phase power electronic load system. In this control method, first three-phase voltages E_abc are generated by the test-inverter as shown in Fig. 2.

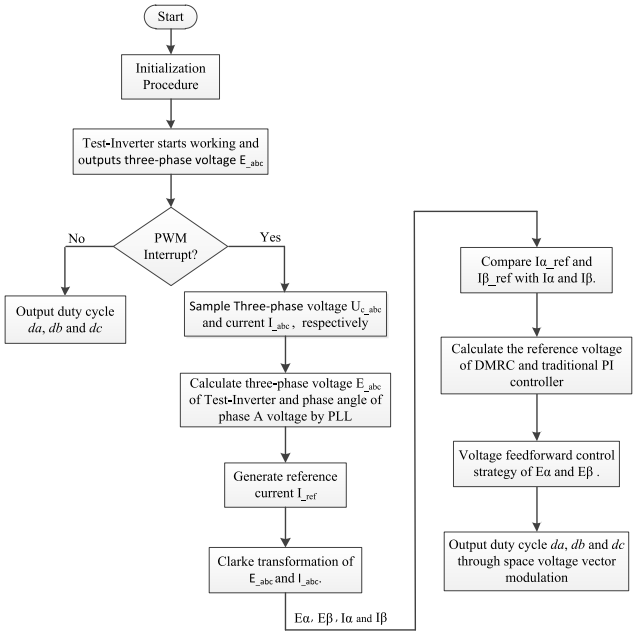

FIGURE 3. Flow chart of the proposed DMRC current control method in the three-phase power electronic load.

Then a condition block is passed to decide whether PWM interrupt is needed. If PWM interrupt hasn't started yet, which means the last PWM cycle has not ended; the gate signals for power switches (da, db and dc) remain unchanged. However, if the interruption comes, then the duty ratios (da, db and dc) are recalculated and redistributed according to Fig. 2 (b).

B. THREE-PHASE PLL SYSTEM

In order to improve the stability of the entire three-phase power electronic load system, accurate and fast information of the phase angle of the driving inverter terminal voltages is essential. The popular method called phase-locked loop (PLL) discussed in [8], [35], [35] is utilized to estimate the synchronization and frequency of a three-phase voltage in this work as presented in Fig. 4.

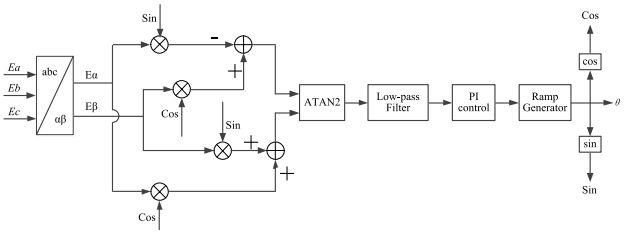

FIGURE 4. Closed-loop control scheme of the PLL.

In order to obtain the voltage frequency ω and the angular position θ of three-phase driving inverter voltages, a PLL is utilized. The PLL is implemented by the ArcTan2-type algorithm and is shown in Fig. 4.

The inputs parameter of PLL block are the three-phase voltages of the tested inverter, and then transformed to stationary reference frame in α-β coordinates. The output of the proportional-integral (PI) controller is used to produce accurate information of the tested inverter by a ramp generator. The closed-loop control scheme of the PLL could reduce frequency ripple and maintain a phase-lock to the three-phase tested inverter voltages. Fig. 5 shows the simulated behavior of PLL when the phase voltage amplitude of the driving inverter varies from 188V to 94V. It can be seen that the main advantage of the PLL has a high accuracy of the angular position under different magnitude of the test-inverter output voltage.

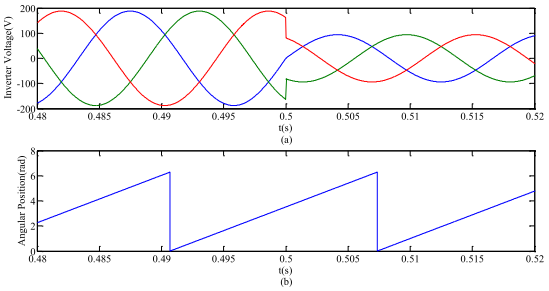

FIGURE 5. PLL response to varying magnitude of the driving inverter output voltage.

III. DMRC CONTROL SCHEME FOR THE THREE-PHASE POWER ELECTRONIC LOAD

A. PROBLEM FORMULATION

Fig. 6 shows a LCL-type filter is used to connect the three-phase test-inverter and simulation converter in this paper. The model of the simulation converter shown in Fig. 6 is given as

$$\frac{d}{dt}\begin{bmatrix} I_{e\_ab}(t) \\ I_{e\_bc}(t) \\ I_{e\_ca}(t) \end{bmatrix} = \frac{R_C}{L1}\begin{bmatrix} I_{ab}(t) \\ I_{bc}(t) \\ I_{ca}(t) \end{bmatrix} - \frac{R_L + R_C}{L1}\begin{bmatrix} I_{e\_ab}(t) \\ I_{e\_bc}(t) \\ I_{e\_ca}(t) \end{bmatrix} - \frac{1}{L1}\begin{bmatrix} U_{c\_ab}(t) \\ U_{c\_bc}(t) \\ U_{c\_ca}(t) \end{bmatrix} + \frac{U_{dc}}{L1}\begin{bmatrix} da(t) \\ db(t) \\ dc(t) \end{bmatrix} \quad (1)$$

$$\frac{d}{dt}\begin{bmatrix} I_{ab}(t) \\ I_{bc}(t) \\ I_{ca}(t) \end{bmatrix} = \frac{R_C}{L2}\begin{bmatrix} I_{e\_ab}(t) \\ I_{e\_bc}(t) \\ I_{e\_ca}(t) \end{bmatrix} - \frac{R_E + R_C}{L2}\begin{bmatrix} I_{ab}(t) \\ I_{bc}(t) \\ I_{ca}(t) \end{bmatrix}$$

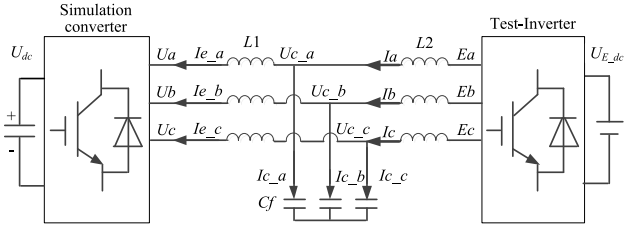

FIGURE 6. The main circuit of the three-phase power electronic load system.

$$+\frac{1}{L2}\begin{bmatrix} U_{c\_ab}(t) \\ U_{c\_bc}(t) \\ U_{c\_ca}(t) \end{bmatrix} - \frac{1}{L2}\begin{bmatrix} E_{\_ab}(t) \\ E_{\_bc}(t) \\ E_{\_ca}(t) \end{bmatrix} \quad (2)$$

$$\frac{d}{dt}\begin{bmatrix} U_{c\_ab}(t) \\ U_{c\_bc}(t) \\ U_{c\_ca}(t) \end{bmatrix} = \frac{1}{C_f}\begin{bmatrix} I_{e\_ab}(t) \\ I_{e\_bc}(t) \\ I_{e\_ca}(t) \end{bmatrix} - \frac{1}{C_f}\begin{bmatrix} I_{ab}(t) \\ I_{bc}(t) \\ I_{ca}(t) \end{bmatrix} \quad (3)$$

where RL, RC, and RE are the parasitic resistances of $L1$, Cf, and $L2$. da, db, and dc are the control signals of simulation converter. In (1)-(3), I_{e_ab} means I_{e_a} minus I_{e_b}, I_{ab} means I_a minus I_b, etc. the phase currents and voltages are used instead of the line currents and phase voltage.

The three-phase converter can be controlled in the α-β coordinate system. The CLARKE transformation matrix from the a-b-c stationary coordinate system to the α-β stationary coordinate system and its inverse transformation matrix are shown in (4).

$$T_{abc\to\alpha\beta} = \frac{2}{3}\begin{bmatrix} 1 & -\frac{1}{2} & -\frac{1}{2} \\ 0 & \frac{\sqrt{3}}{2} & -\frac{\sqrt{3}}{2} \end{bmatrix}, \quad T_{\alpha\beta\to abc} = \begin{bmatrix} 1 & 0 \\ -\frac{1}{2} & \frac{\sqrt{3}}{2} \\ -\frac{1}{2} & -\frac{\sqrt{3}}{2} \end{bmatrix} \quad (4)$$

The implementation of control in the α-β static coordinate system is beneficial to simplifying the control algorithm and improving its reliability. According to Fig. 6, the mathematical model of the main part circuit in the stationary α-β frame can be expressed as

$$\frac{d}{dt}\begin{bmatrix} I_{e\_\alpha}(t) \\ I_{e\_\beta}(t) \end{bmatrix} = \frac{R_C}{L1}\begin{bmatrix} I_\alpha(t) \\ I_\beta(t) \end{bmatrix} - \frac{R_L + R_C}{L1}\begin{bmatrix} I_{e\_\alpha}(t) \\ I_{e\_\beta}(t) \end{bmatrix} - \frac{1}{L1}\begin{bmatrix} U_{c\_\alpha}(t) \\ U_{c\_\beta}(t) \end{bmatrix} + \frac{U_{dc}}{L1}\begin{bmatrix} d_\alpha(t) \\ d_\beta(t) \end{bmatrix} \quad (5)$$

$$\frac{d}{dt}\begin{bmatrix} I_\alpha(t) \\ I_\beta(t) \end{bmatrix} = \frac{R_C}{L2}\begin{bmatrix} I_{e\_\alpha}(t) \\ I_{e\_\beta}(t) \end{bmatrix} - \frac{R_C + R_E}{L2}\begin{bmatrix} I_\alpha(t) \\ I_\beta(t) \end{bmatrix} + \frac{1}{L2}\begin{bmatrix} U_{c\_\alpha}(t) \\ U_{c\_\beta}(t) \end{bmatrix} - \frac{1}{L2}\begin{bmatrix} E\alpha(t) \\ E\beta(t) \end{bmatrix} \quad (6)$$

$$\frac{d}{dt}\begin{bmatrix} U_{c\_\alpha}(t) \\ U_{c\_\beta}(t) \end{bmatrix} = \frac{1}{C_f}\begin{bmatrix} I_{e\_\alpha}(t) \\ I_{e\_\beta}(t) \end{bmatrix} - \frac{1}{C_f}\begin{bmatrix} I_\alpha(t) \\ I_\beta(t) \end{bmatrix} \quad (7)$$

where I_{e_α}, I_{e_β} are phase currents of the α, β axis in the side of simulation converter, respectively. U_{c_α}, U_{c_β} are α, β axis capacitance voltages, respectively. $E\alpha$, $E\beta$ are α, β axis voltages of the test-inverter side, respectively. $I\alpha$, $I\beta$ are α, β axis currents of the test-inverter side, respectively. $d\alpha$, $d\beta$ are α, β axis control signals of the simulation converter side, respectively.

The control objective of the three-phase power electronic load system is to make phase currents of the test-inverter side precise tracking the reference current $I_{\alpha\beta\_ref}$. Hence, a plug-in DMRC controller is developed to accurately track the calculated reference current in the α-β stationary reference frame, which will be detailed description next.

B. DESIGN OF PLUG-IN DMRC CONTROLLER

The block diagram of a plug-in DMRC scheme is shown in Fig. 7. G_p(z) is the transfer function of simulation converter

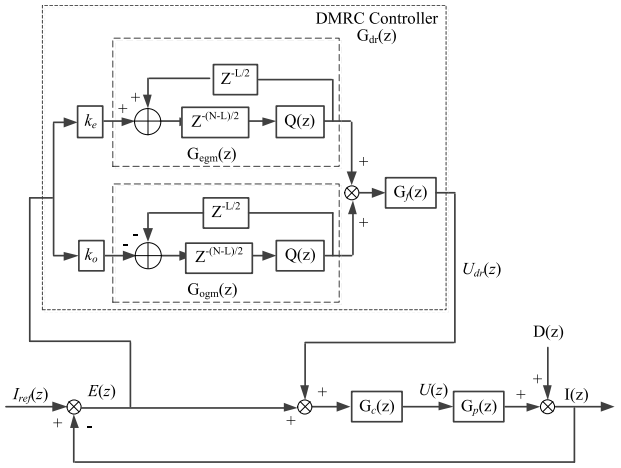

FIGURE 7. Block diagram of DMRC scheme.

and LCL filter; G_c(z) is the transfer function of the conventional PI control for fundamental current regulation; $z^{-N/2}$ is the integer period delay; Q(z) and G_f(z) are filters to improve robustness of the whole system; I(z) is the driving inverter output current injected into the three-phase power electronic load system; I_{ref}(z) is the reference current of test-inverter terminal; and D(z) is the disturbance of test-inverter current.

The conventional control system without DMRC can be expressed by

$$H(z) = \frac{G_c(z)G_p(z)}{1 + G_c(z)G_p(z)} \quad (8)$$

As shown in Fig. 7, a general dual-mode-structure prototype RC controller G_{dr}(z) can be expressed as

$$G_{dr}(z) = \left(k_o G_{ogm}(z) + k_e G_{egm}(z)\right) G_f(z) \quad (9)$$

$$= \left(k_o \frac{-z^{-N/2}Q(z)}{1 + z^{-N/2}Q(z)} + k_e \frac{z^{-N/2}Q(z)}{1 - z^{-N/2}Q(z)}\right) \quad (10)$$

where $N = f_s/f_0$ with $f_0 = \omega_0 / 2\pi$ being the fundamental frequency of the signals and fs being the sampling rate, respectively. N is an even integer. G_{ogm}(z) is an even-harmonic signal generator, G_{egm}(z) is an odd-harmonic signal generator, k_o is an odd-harmonic gain, k_e is an even-harmonic gain[37], [38].

The closed-loop transfer function of the DMRC system in Fig. 7 is

$$\frac{I(z)}{I_{ref}(z)} = \frac{H(z)\left(1 + G_f(z)\left(k_o G_{ogm}(z) + k_e G_{egm}(z)\right)\right)}{1 + H(z)G_f(z)\left(k_o G_{ogm}(z) + k_e G_{egm}(z)\right)} \quad (11)$$

According to the stability theory of discrete system, the closed-loop DMRC system as shown in Fig. 7 is asymptotically stable if the following conditions are fulfilled.

1. all the roots of $1 + G_c(z)\, G_p(z) = 0$ are inside the unit circle;

2. $0 < H(z)\, G_f(z) \le 1$;

3. $k_o + k_e < 2/(1 + \varepsilon)$, $k_o \ge 0$, $k_e \ge 0$, and ε being a positive constant.

In order to obtain the characteristics of zero phase shift and zero gain, $G_f(z)$ is usually chosen as the reverse model of $H(z)$ [17], [36]. However, in practice application, due to uncertainties system model, dead-time and parameter variation, it is not feasible to obtain the exact model of $H(z)$. That is, the practical reverse model of $G_f(z)$ of $H(z)$ can be expressed as

$$G_f(z) = G_{fn}(z)\,(1 + \Delta(z)) \tag{12}$$

where $H(z)$ $G_{fn}(z) = 1$, $\Delta(z)$ represents the uncertainties when it is considered to be stable and bounded by $|\Delta(e^{j\omega})| \le \varepsilon$.

C. PERFORMANCE ANALYSIS OF PLUG-IN DMRC CONTROLLER

The transfer function from disturbance signal to error signal in Fig. 7 is

$$\frac{E(z)}{D(z)} = 1 - \frac{\left(1 + G_c(z)G_p(z)\right)^{-1}}{1 + H(z)G_f(z)\left(k_o G_{ogm}(z) + k_e G_{egm}(z)\right)} \tag{13}$$

From Fig. 7, the error transfer function M(z) from reference current signal I_{ref} (z) minus disturbance signal $D(z)$ to current steady-state error $E(z)$ for the plug-in DMRC system can be derived as

$$E(z) = M(z)\left(I_{ref}(z) - D(z)\right) \tag{14}$$

$$= \frac{1}{1 + \mathrm{G}_c(z)\mathrm{G}_p(z)} \frac{1}{1 + H(z)G_{dr}(z)} \left(I_{ref}(z) - D(z)\right) \tag{15}$$

From (12), we can obtained

$$G_f(z)H(z) = G_{fn}(z)H(z)\,(1 + \Delta(z)) = 1 + \Delta(z) \tag{16}$$

Then the formula in (15) can be expressed as

$$E(z) = \frac{1}{1 + \mathrm{G}_c(z)\mathrm{G}_p(z)} \frac{1}{\mathrm{G}_{\mathrm{x}}(z) + (1 + \Delta(z))G_y(z)} \times \left(I_{ref}(z) - D(z)\right) \tag{17}$$

where

$$G_x(z) = 1 - z^{-N}Q^2(z) \tag{18}$$

$$G_y(z) = (k_o + k_e)z^{-N}Q^2(z) + (k_e - k_o)z^{-N/2}Q(z) \tag{19}$$

If the DMRC system in Fig. 7 with gains $k_o = k_e = k_r/2$, then (15) can be derived as

$$E(z) = \frac{\left(1 - z^{-N}Q^2(z)\right)(1 - H(z))}{1 - z^{-N}Q^2(z)(1 - k_r G_f(z)H(z))} \left(I_{ref}(z) - D(z)\right) \tag{20}$$

Obviously, if $|Q^2(z)(1 - k_r G_f(z)H(z))| < 1$, then all poles are inside the unit circle. The transfer function (20) is asymptotically stable, when $H(z)$ is stable.

When $Q(z)$=1, if $H(z)$ and $G_f(z)$ are asymptotically stable, it is clear that the tracking error and disturbance error can be attenuated. The steady-state tracking performance of the three-phase power electronic load system is improved by combing DMRC controller.

D. PARAMETER DESIGN OF PLUG-IN DMRC CONTROLLER

The tracking accuracy, output THD and stability region of a high-performance DMRC controller is depended on $Q(z)$, $G_f(z)$ and the relationship between various parameters and $H(z)$ in the design.

1) DESIGN OF ATTENUATION FILTER Q(Z) AND Z^{-N}

The function z^{-N} represents N delay units. N is the number of samples in one repetitive reference period. For example, the controller with a sampling frequency $fs = 10kHz$ is used to generate a fundamental current frequency $50Hz$ in a DMRC system, $N = 10kHz/50Hz = 200$. Usually, a constant $Q(z)$ is adopted to improve the robustness and stability of a system. According to engineering experience, $Q(z)$ is set to 0.95.

2) DESIGN OF CORRECTOR GF(Z)

In order to maintain good effects at medial and low frequencies performance, and provide sufficient high frequency attenuation, the corrector $G_f(z)$ can be designed in plug-in DMRC system.

To enhance the system stability, a conventional second-order low-pass filter $G_f(z)$ is adopted, which is suitable for high frequencies attenuation, and simplifying the controller design. The transfer function of second-order filter G_f (s) can be derived according to the inverter plant and damping ratio.

$$G_f(\mathrm{s}) = \frac{1}{(L_1 + L_2)\,C_f s^2 + K_d s + 1} \tag{21}$$

$$\xi = \frac{K_d}{2\sqrt{(L_1 + L_2)\,C_f}} \tag{22}$$

$$s = \frac{2}{T_s}\frac{z - 1}{z + 1} \tag{23}$$

G_f (z) is the discrete time domain expression of the Tustin Euler. According to (21)-(23), It is obtained as

$$G_f(z) = \frac{0.0493z^2 + 0.0987z + 0.0493}{z^2 - 1.285z + 0.483} \tag{24}$$

The design of G_f (z) is appropriate for suppressing the high frequency resonant. The three-phase power electronic load system can be corrected and compensated by G_f (z). The bode plots of G_{cp} (z) G_f (z) is shown in Fig. 8. Fig. 8 shows that the resonance frequency peak attenuated and the high frequency amplitude decreases rapidly.

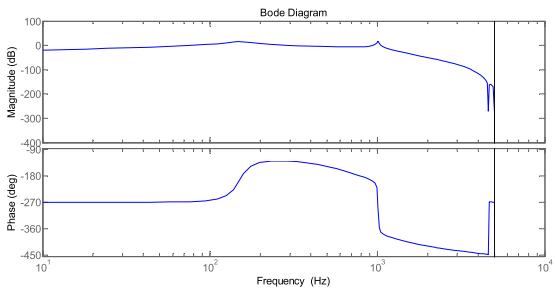

FIGURE 8. Frequency characteristics of $G_{cp}(z)G_f(z)$.

It can be seen from Fig. 8, although the gain of G_{cp} (z) Gf (z) has a good performance in high frequencies attenuation, the system has a large phase lag. In order to compensate the phase lag, an advance compensation element z^{10} is adopted. It can guarantees ideal tracking accuracy and phase compensation at media and low frequencies.

IV. SIMULATION RESULTS

Based on the above analysis, simulations of three-phase power electronics load are carried out using various modules of MATLAB/Simulink tool box in this section. In order to validate effectiveness of the proposed current control strategy, simulation results are presented with three different control strategies on the three-phase electronics load system for comparison. The amplitude of the phase reference current is 10A.

A. STEADY-STATE PERFORMANCE

In this sub-section, the steady-state responses for the three different current tracking methods are presented to verify the current tracking performance of plug-in DMRC strategy. Fig. 9, 11, and 13 show the steady-state responses of A-phase current in the three-phase electronics load system under different AC frequencies, respectively. Fig 10, 12, and 14 show the A-phase current spectrum of three-phase electronics load system under different tested-inverter AC frequencies, respectively.

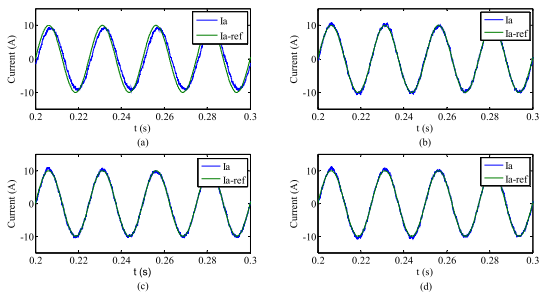

FIGURE 9. Steady-state performance of A-phase current in three-phase power electronics load system at 40Hz. (a) under the conventional PI control strategy, (b) under CRC strategy, (c) under DMRC strategy with gains $k_o = 0.5$ and $k_e = 1$, and (d) under DMRC strategy with gains $k_o = 1$ and $k_e = 0.5$.

As seen in Fig. 9, the three-phase electronics load is operated at 40Hz. Figs. 9(a) shows the steady-state response of A-phase current utilizing the conventional PI control strategy. It is difficult to meet the requirements of current tracking accuracy by the PI control strategy in Fig. 9(a). It can be observed that the A-phase current can track the reference current well in Fig. 9(b), (c), and (d). The A-phase current THD is 1.90% with the conventional PI control strategy at 40Hz in Fig. 10(a). The A-phase current THD is 1.84% with the CRC strategy at 40Hz in Fig. 10(b). However, when the plug-in DMRC controller with gains $k_o = 0.5$ and $k_e = 1$ is adopted in the three-phase electronics load system, the A-phase current THD is 1.04% in Fig. 10(c). When the plug-in DMRC controller with gains $k_o = 1$ and $k_e = 0.5$ is adopted in the three-phase electronics load system, the A-phase current THD is 1.16% in Fig. 10(d).

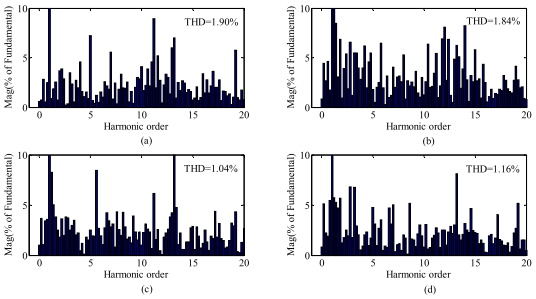

FIGURE 10. The A-phase current spectrum of three-phase power electronics load system at 40Hz. (a) under the conventional PI control strategy, (b) under CRC strategy, (c) under DMRC strategy with gains $k_o = 0.5$ and $k_e = 1$, and (d) under DMRC strategy with gains $k_o = 1$ and $k_e = 0.5$.

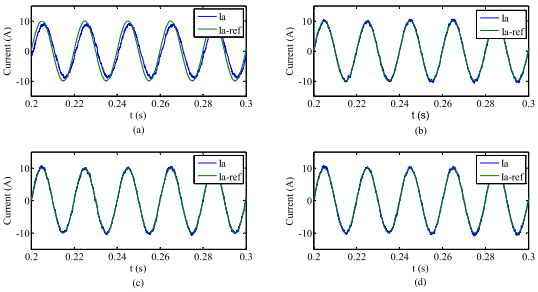

FIGURE 11. Steady-state performance of A-phase current in three-phase power electronics load system at 50Hz. (a) Under the conventional PI control strategy, (b) under CRC strategy, (c) under DMRC strategy with gains $k_o = 0.5$ and $k_e = 1$, and (d) under DMRC strategy with gains $k_o = 1$ and $k_e = 0.5$.

Fig. 11 is the three-phase power electronics load operating at 50Hz. It can be seen that the tracking accuracy of A-phase current under the conventional PI control strategy is poor in Fig. 11(a). The current tracking accuracy of RC and DMRC strategy are better than that of conventional PI control strategy. For the conventional PI control strategy, the A-phase current THD is 1.94% in Fig. 12(a). For CRC control strategy, the A-phase current THD is 1.65% in Fig. 12(b). For the plug-in DMRC controller with gains $k_o = 0.5$ and $k_e = 1$, the A-phase current THD is 1.560% in Fig. 12(c). For the plug-in DMRC controller with gains $k_o = 1$ and $k_e = 0.5$, the A-phase current THD is 1.78% in Fig. 12(d).

In Fig. 13, it can be observed that the current tracking accuracy of CRC strategy is better than that of conventional PI strategy at 60Hz. For the DMRC proposed in this paper, the current tracking accuracy and current spectrum is worse than that of CRC strategy at 60Hz. Fig. 14 shows the A-phase current spectrum of three-phase PEL system at 60Hz. The THD of conventional PI controller is 1.85% under 60Hz in Fig. 14(a). The THD of CRC control strategy is 1.80% at 60Hz in Fig. 14(b). The THD of DMRC strategy with gains $k_o = 0.5$ and $k_e = 1$ is 1.56% at 60Hz in Fig. 14(c). The THD of DMRC strategy with gains $k_o = 1$ and $k_e = 0.5$ is 1.42% at 60Hz in Fig. 14(d).

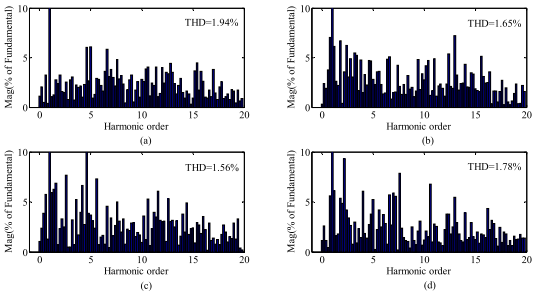

FIGURE 12. The A-phase current spectrum of three-phase power electronics load system at 50Hz. (a) Under the conventional PI control strategy, (b) under CRC strategy, (c) under DMRC strategy with gains $k_o = 0.5$ and $k_e = 1$, and (d) under DMRC strategy with gains $k_o = 1$ and $k_e = 0.5$.

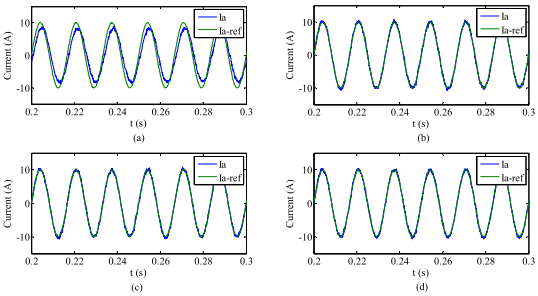

FIGURE 13. Steady-state performance of A-phase current in three-phase power electronics load system at 60Hz. (a) Under the conventional PI control strategy, (b) under CRC strategy, (c) under DMRC strategy with gains $k_o = 0.5$ and $k_e = 1$, and (d) under DMRC strategy with gains $k_o = 1$ and $k_e = 0.5$.

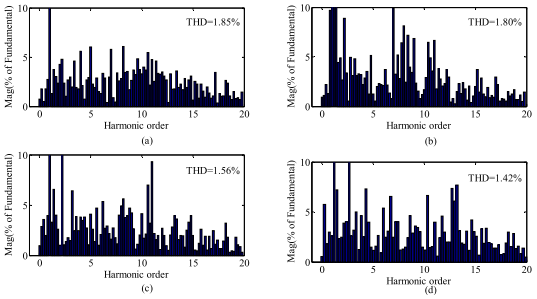

FIGURE 14. The A-phase current spectrum of three-phase power electronics load system at 60Hz. (a) Under the conventional PI control strategy, (b) under CRC strategy, (c) under DMRC strategy with gains $k_o = 0.5$ and $k_e = 1$, and (d) under DMRC strategy with gains $k_o = 1$ and $k_e = 0.5$.

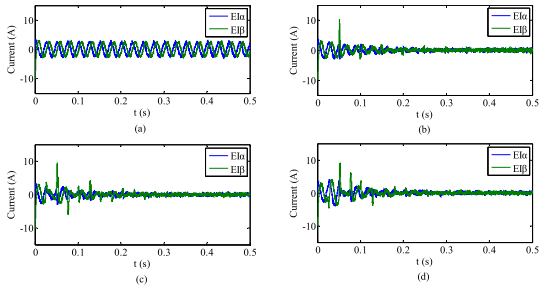

FIGURE 15. The error waveforms of $\alpha\beta$-axis currents in three-phase power electronics load system at 40Hz. (a) Under the conventional PI control strategy, (b) under CRC strategy, (c) under DMRC strategy with gains $k_o = 0.5$ and $k_e = 1$, and (d) under DMRC strategy with gains $k_o = 1$ and $k_e = 0.5$.

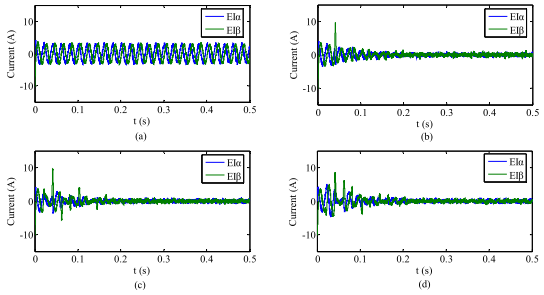

FIGURE 16. The error waveforms of $\alpha\beta$-axis currents in three-phase power electronics load system at 50Hz. (a) Under the conventional PI control strategy, (b) under CRC strategy, (c) under DMRC strategy with gains $k_o = 0.5$ and $k_e = 1$, and (d) under DMRC strategy with gains $k_o = 1$ and $k_e = 0.5$.

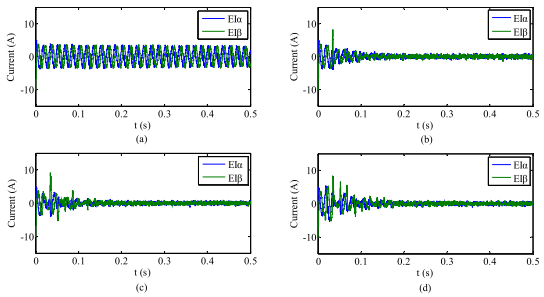

FIGURE 17. The error waveforms of $\alpha\beta$-axis currents in three-phase power electronics load system at 60Hz. (a) Under the conventional PI control strategy, (b) under CRC strategy, (c) under DMRC strategy with gains $k_o = 0.5$ and $k_e = 1$, and (d) under DMRC strategy with gains $k_o = 1$ and $k_e = 0.5$.

Therefore, the plug-in dual-mode structure repetitive control strategy achieves higher current tracking accuracy than conventional PI strategy and CRC strategy do under different AC frequency.

B. TRANSIENT RESPONSE

In addition to the study of steady-state response, the transient performance is further researched. Fig. 14-17 illustrate the dynamic response to step-change of current by tracking the current error EIα and EIβ in the α-β stationary reference frame at 40Hz, 50Hz, 60Hz, respectively.

As seen in Fig. 15(a), 16(a), and 17(a), due to the conventional PI controller is difficult at tracking AC current command, the $\alpha\beta$-axis currents errors are significant large, which lead to heavily distorted and harmonics in the output current. On analyzing the waveforms of Fig. 15(b), 16(b), and 17(b), it can be seen that the steady-state error waveforms of $\alpha\beta$-axis currents are reduced from $\pm$10A to $\pm$1A under the CRC strategy, which are a little worse than that of$\alpha\beta$-axis currents under DMRC control strategy.

Fig. 15-17 illustrate that, in terms of such a current tracking error convergence rate, the performance of the DMRC

strategy with gains $k_o = 0.5$ and $k_e = 1$ is better than that of the DMRC strategy with gains $k_o = 1$ and $k_e = 0.5$.

V. CONCLUSION

In this paper, a novel current control method based on plug-in DMRC has been presented for three-phase power electronic load. The proposed plug-in DMRC reduces the time delay to half of the fundamental period and significantly improves the transient response performance when compared with the conventional repetitive control scheme. Moreover, a phase lead compensation is incorporated into the proposed plug-in DMRC method, which is benefit to the overall system to be stable with a large gain. A low pass filter Q(z) is designed to improve the robustness of the overall system. The feasibility and effectiveness of the proposed current control method are validated through simulation for three-phase power electronic load system, As a result, when the proposed method is applied, the AC current total harmonic distortion (THD) is reduced to less than 1.8%, It can provides nearly 20% and 10% reduction in THD of phase current when compared with PI controller and conventional RC method, respectively. The plug-in DMRC method achieves a better tracking accuracy than the CRC method does with $k_o = 2k_e$ when AC frequency is below 50Hz in a three-phase AC systems. When AC frequency is exceed 50Hz in a three-phase AC systems, the plug-in DMRC method achieves a better tracking accuracy than the CRC method does with $2k_o = k_e$. The tracking error convergence rate of plug-in DMRC is faster than the CRC does when $k_o \geq 2k_e$ in a three-phase AC systems

REFERENCES

[1] K. Saito and H. Akagi, "A real-time real-power emulator of a medium-voltage high-speed induction motor loaded with a centrifugal compressor," *IEEE Trans. Ind. Appl.*, vol. 55, no. 5, pp. 4821–4833, Sep. 2019.

[2] O. Vodyakho, M. Steurer, C. S. Edrington, and F. Fleming, "An induction machine emulator for high-power applications utilizing advanced simulation tools with graphical user interfaces," *IEEE Trans. Energy Convers.*, vol. 27, no. 1, pp. 160–172, Mar. 2012.

[3] A. Schmitt, M. Gommeringer, M. Braun, J. Richter, and T. Wersal, "A novel 100 kW power hardware-in-the-loop emulation test bench for permanent magnet synchronous machines with nonlinear magnetics," in *Proc. 8th IET Int. Conf. Power Electron., Mach. Drives (PEMD)*, 2016, pp. 1–6.

[4] H. J. Slater, D. J. Atkinson, and A. G. Jack, "Real-time emulation for power equipment development. II. The virtual machine," *IEE Proc.-Electr. Power Appl.*, vol. 145, no. 3, pp. 153–158, May 1998.

[5] A. Schmitt, J. Richter, U. Jurkewitz, and M. Braun, "FPGA-based real-time simulation of nonlinear permanent magnet synchronous machines for power hardware-in-the-loop emulation systems," in *Proc. IECON 40th Annu. Conf. IEEE Ind. Electron. Soc.*, Oct. 2014, pp. 3763–3769.

[6] R. S. Kaarthik and P. Pillay, "Emulation of a permanent magnet synchronous generator in real-time using power hardware-in-the-loop," in *Proc. IEEE Int. Conf. Power Electron., Drives Energy Syst. (PEDES)*, Dec. 2016, pp. 1–6.

[7] Y. S. Rao and M. C. Chandorkar, "Real-time electrical load emulator using optimal feedback control technique," *IEEE Trans. Ind. Electron.*, vol. 57, no. 4, pp. 1217–1225, Apr. 2010.

[8] M. A. Masadeh, K. S. Amitkumar, and P. Pillay, "Power electronic converter-based induction motor emulator including main and leakage flux saturation," *IEEE Trans. Transport. Electrific.*, vol. 4, no. 2, pp. 483–493, Jun. 2018.

[9] A. Hoke, S. Chakraborty, and T. Basso, "A power hardware-in-the-loop framework for advanced grid-interactive inverter testing," in *Proc. IEEE Power Energy Soc. Innov. Smart Grid Technol. Conf. (ISGT)*, Feb. 2015, pp. 1–5.

[10] C. S. Edrington, M. Steurer, J. Langston, T. E. Mezyani, and K. Schoder, "Characteristics and design of power hardware-in-the-loop simulations for electrical power systems," *IEEE Trans. Ind. Electron.*, vol. 63, no. 1, pp. 406–417, Jan. 2016.

[11] P. Kotsampopoulos, A. Kapetanaki, G. Messinis, V. Kleftakis, and N. Hatziargyriou, "A PHIL facility for microgrids," *Int. J. Distrib. Energy Resour.*, vol. 9, no. 1, pp. 71–86, Mar. 2013.

[12] J. Wang, L. Yang, Y. Ma, X. Shi, X. Zhang, L. Hang, K. Lin, L. M. Tolbert, F. Wang, and K. Tomsovic, "Regenerative power converters representation of grid control and actuation emulator," in *Proc. IEEE Energy Convers. Congr. Expo. (ECCE)*, Sep. 2012, pp. 2460–2465.

[13] J. Wang, Y. Ma, L. Yang, L. M. Tolbert, and F. Wang, "Power converter-based three-phase induction motor load emulator," in *Proc. 28th Annu. IEEE Appl. Power Electron. Conf. Expo. (APEC)*, Mar. 2013, pp. 3270–3274.

[14] W. Ren, M. Steurer, and T. L. Baldwin, "Improve the stability and the accuracy of power hardware-in-the-loop simulation by selecting appropriate interface algorithms," *IEEE Trans. Ind. Appl.*, vol. 44, no. 4, pp. 1286–1294, Jul. 2008.

[15] T. Ould-Bachir, C. Dufour, J. Belanger, J. Mahseredjian, and J. P. David, "Effective floating-point calculation engines intended for the fpga-based hil simulation," in *Proc. IEEE Int. Symp. Ind. Electron.*, May 2012, pp. 1363–1368.

[16] B. Asghari and V. Dinavahi, "Experimental validation of a geometrical nonlinear permeance network based real-time induction machine model," *IEEE Trans. Ind. Electron.*, vol. 59, no. 11, pp. 4049–4062, Nov. 2012.

[17] M. Tomizuka, T. Tsao, and K. Chew, "Analysis and synthesis of discrete-time repetitive controllers," *Trans. ASME, J. Dyn. Syst., Meas. Control*, vol. 110, pp. 271–280, Sep. 1988.

[18] A. Griffo, D. Salt, R. Wrobel, and D. Drury, "Computationally efficient modelling of permanent magnet synchronous motor drives for real-time hardware-in-the-loop simulation," in *Proc. 39th Annu. Conf. IEEE Ind. Electron. Soc.*, Nov. 2013, pp. 5368–5373.

[19] C. Dufour, S. Cense, T. Yamada, R. Imamura, and J. Belanger, "FPGA permanent magnet synchronous motor floating-point models with variable-DQ and spatial harmonic finite-element analysis solvers," in *Proc. 15th Int. Power Electron. Motion Control Conf. (EPE/PEMC)*, Sep. 2012, p. LS6b.

[20] Y. Ma, Y. Yu, Q. Yan, and J. Cai, "Dual-period repetitive control for nonparametric uncertain systems with deadzone input," *IEEE Access*, vol. 7, pp. 165488–165495, 2019.

[21] X. Zhang and Z. Zheng, "Application of repetitive control in electric spring," *IEEE Access*, vol. 8, pp. 216607–216616, 2020.

[22] Z. Chen, H. Zha, K. Peng, J. Yang, and J. Yan, "A design method of optimal PID-based repetitive control systems," *IEEE Access*, vol. 8, pp. 139625–139633, 2020.

[23] A. Monti, S. D'Arco, and A. Deshmukh, "A new architecture for low cost power hardware in the loop testing," in *Proc. IEEE Int. Symp. Ind. Electron.*, Jun. 2008, pp. 2183–2188.

[24] F. Alvarez-Gonzalez, A. Griffo, B. Sen, and J. Wang, "Real-time hardware-in-the-loop simulation of permanent-magnet synchronous motor drives under stator faults," *IEEE Trans. Ind. Electron.*, vol. 64, no. 9, pp. 6960–6969, Sep. 2017.

[25] P. Schulting, C. H. van der Broeck, and R. W. De Doncker, "Analysis and design of repetitive controllers for applications in distorted distribution grids," *IEEE Trans. Power Electron.*, vol. 34, no. 1, pp. 996–1004, Jan. 2019.

[26] K. Zhou, K.-S. Low, D. Wang, F.-L. Luo, B. Zhang, and Y. Wang, "Zero-phase odd-harmonic repetitive controller for a single-phase PWM inverter," *IEEE Trans. Power Electron.*, vol. 21, no. 1, pp. 193–201, Jan. 2006.

[27] D. del Puerto-Flores, J. M. A. Scherpen, M. Liserre, M. M. J. de Vries, M. J. Kransse, and V. G. Monopoli, "Passivity-based control by series/parallel damping of single-phase PWM voltage source converter," *IEEE Trans. Control Syst. Technol.*, vol. 22, no. 4, pp. 1310–1322, Jul. 2014.

[28] R. Grino, R. Cardoner, R. Costa-Castello, and E. Fossas, "Digital repetitive control of a three-phase four-wire shunt active filter," *IEEE Trans. Ind. Electron.*, vol. 54, no. 3, pp. 1495–1503, Jun. 2007.

[29] R. I. Bojoi, L. R. Limongi, D. Roiu, and A. Tenconi, "Enhanced power quality control strategy for single-phase inverters in distributed generation systems," *IEEE Trans. Power Electron.*, vol. 26, no. 3, pp. 789–806, Mar. 2011.
[30] S. Jiang, D. Cao, Y. Li, J. Liu, and F. Z. Peng, "Low-THD, fast-transient, and cost-effective synchronous-frame repetitive controller for three-phase UPS inverters," *IEEE Trans. Power Electron.*, vol. 27, no. 6, pp. 2994–3005, Jun. 2012.
[31] K. Zhou, D. Wang, B. Zhang, Y. Wang, J. A. Ferreira, and S. W. H. de Haan, "Dual-mode structure digital repetitive control," *Automatica*, vol. 43, no. 3, pp. 546–554, Mar. 2007.
[32] B. Chandrasekar, C. Nallaperumal, S. Padmanaban, M. S. Bhaskar, J. B. Holm-Nielsen, Z. Leonowicz, and S. O. Masebinu, "Non-isolated high-gain triple port DC–DC buck-boost converter with positive output voltage for photovoltaic applications," *IEEE Access*, vol. 8, pp. 113649–113666, 2020.
[33] S. A. Gorji, H. G. Sahebi, M. Ektesabi, and A. B. Rad, "Topologies and control schemes of bidirectional DC–DC power converters: An overview," *IEEE Access*, vol. 7, pp. 117997–118019, 2019.
[34] A. Sharma, S. S. Nag, G. Bhuvaneswari, and M. Veerachary, "An improved mode transition technique for a non-isolated bidirectional DC-DC converter," *IEEE Trans. Circuits Syst. II, Exp. Briefs*, vol. 67, no. 12, pp. 3093–3097, Dec. 2020.
[35] S. K. Chung, "Phase-locked loop for grid-connected three-phase power conversion systems," *IEE Proc. Electr. Power Appl.*, vol. 147, no. 3, pp. 213–219, May 2000.
[36] R. Costa-Castelló, R. Griñó, and E. Fossas, "Odd-harmonic digital repetitive control of a single-phase current active filter," *IEEE Trans. Power Electron.*, vol. 19, no. 4, pp. 1060–1068, Jul. 2004.
[37] Z. Keliang, W. Danwei, Z. Bin, and W. Yigang, "Dual-mode structure repetitive control," in *Proc. Chin. Control Conf.*, Jul. 2006, pp. 525–529.
[38] K. Zhou, D. Wang, B. Zhang, and Y. Wang, "Plug-in dual-mode-structure repetitive controller for CVCF PWM inverters," *IEEE Trans. Ind. Electron.*, vol. 56, no. 3, pp. 784–791, Mar. 2009.
[39] P. Cui, G. Zhang, Z. Liu, B. Han, and Q. Wang, "A second-order dual mode repetitive control for magnetically suspended rotor," *IEEE Trans. Ind. Electron.*, vol. 67, no. 6, pp. 4946–4956, Jun. 2020.
[40] Z. Zou, Z. Wang, M. Cheng, and Y. Yang, "Active power filter for harmonie compensation using a digital dual-mode-structure repetitive control approach," in *Proc. 3rd IEEE Int. Symp. Power Electron. Distrib. Gener. Syst. (PEDG)*, Jun. 2012, pp. 161–166.
[41] J. Li, G. Liu, P. Cui, S. Zheng, and X. Chen, "3/2-order dual-mode fractional repetitive control for harmonic vibration suppression in magnetically suspended rotor," *IEEE Sensors J.*, vol. 20, no. 24, pp. 14713–14721, Dec. 2020.
[42] Y. Wang, L. Zheng, H. Zhang, and W. X. Zheng, "Fuzzy observer-based repetitive tracking control for nonlinear systems," *IEEE Trans. Fuzzy Syst.*, vol. 28, no. 10, pp. 2401–2415, Oct. 2020.
[43] W. Shaokun, H. Zhenyi, and P. Chuanbiao, "A repetitive control strategy of AC electronic load with energy recycling," in *Proc. Int. Technol. Innov. Conf. (ITIC)*, 2009, pp. 12–14.
[44] S. Akhlaghi and M. Zolghadri, "Predictive current control for programmable electronic AC load," in *Proc. 11th Power Electron., Drive Syst., Technol. Conf. (PEDSTC)*, Feb. 2020, pp. 1–5.
[45] X. She, Y. Zou, C. Wang, L. Lin, J. Tang, and J. Chen, "Research on power electronic load: Topology, modeling, and control," in *Proc. 24th Annu. IEEE Appl. Power Electron. Conf. Expo.*, Feb. 2009, pp. 1–5.
[46] Z. Geng, D. Gu, T. Hong, and D. Czarkowski, "Programmable electronic AC load based on a hybrid multilevel voltage source inverter," *IEEE Trans. Ind. Appl.*, vol. 54, no. 5, pp. 5512–5522, Sep. 2018.
[47] W. Jiang, X. Zhang, P. Lin, H. Iu, and T. Fernando, "Combined sliding-mode control for the IFDBC interfaced DC microgrids with power electronic loads," *IEEE J. Emerg. Sel. Topics Power Electron.*, vol. 8, no. 4, pp. 3396-3410, Dec. 2020.
[48] J. Tiancheng, Q. Yingchan, and Z. Hongtao, "Research on control strategy of new current-type energy-fed AC electronic load," in *Proc. IEEE Sustain. Power Energy Conf. (iSPEC)*, Nov. 2020, pp. 258–263.
[49] K. S. Amitkumar, R. S. Kaarthik, and P. Pillay, "A versatile power-hardware-in-the-loop-based emulator for rapid testing of transportation electric drives," *IEEE Trans. Transport. Electrific.*, vol. 4, no. 4, pp. 901–911, Dec. 2018.

ZHENG ZHANG received the M.S. degree in electrical engineering from Anhui Polytechnic University, Wuhu, China, in 2016. He is currently pursuing the Ph.D. degree with the Beijing Institute of Technology, Beijing, China.

His research interests include machine drives, power converter control, and high performance control strategy.

XINGHUA LIU received the Ph.D. degree in power machinery and engineering from Beijing Institute of Technology, Beijing, China, in 1996.

He is currently an Associate Professor with the Department of Thermal Energy and Dynamics Engineering, Beijing Institute of Technology. His research interests include the combustion of internal combustion engine and the fields of engine electronic control.

YUE ZHANG received the B.Eng. degree in mechatronic engineering from Changchun University of Science and Technology, China, in 2011. He is currently pursuing the Ph.D. degree in power machinery and engineering with the Beijing Institute of Technology, Beijing, China.

His current research interests include the modeling and simulation of electrochemical systems, battery management systems, and capacity fade.

CHONGBING ZHANG received the B.S. degree from Beijing Institute of Technology, Beijing, China, in 2019, where he is currently pursuing the M.S. degree with the School of Mechanical Engineering.

His research interests include the modeling and design of power electronics circuits, efficient power conversion, and renewable electrical energy systems.

WANGMIN DENG received the B.S. degree in vehicle engineering from China Agricultural University, Beijing, China, in 2019. He is currently pursuing the master's degree with the Beijing Institute of Technology.

His research interests include sliding mode control, intelligent control, evolutionary algorithms, driverless technology, and power converters.